Article:
Schrade, M., Maso, N., Perejon, A. et al. (2017) Defect chemistry and electrical properties of BiFeO3. Journal of Materials Chemistry C (38). pp. 10077-10086. ISSN: 2050-7526

https://doi.org/10.1039/c7tc03345a

Defect chemistry and electrical properties of $BiFeO_3$

Matthias Schrade[1], Nahum Masó[2,5], Antonio Perejón[3,4], Luis A. Pérez-Maqueda[3], and Anthony R. West[5]

[1]Department of Physics, Centre for Materials Science and Nanotechnology, University of Oslo, Sem Sælandsvei 24, 0371 Oslo, Norway.

[2]Department of Chemistry, University of Oslo, FERMiO/SMN, Gaustadalléen 21, 0349 Oslo, Norway.

[3]Instituto de Ciencia de Materiales de Sevilla (CSIC-Universidad de Sevilla), C. Américo Vespucio 49, Sevilla 41092, Spain.

[4]Departamento de Química Inorgánica, Facultad de Química, Universidad de Sevilla, Sevilla 41071, Spain.

[5]Department of Materials Science and Engineering, The University of Sheffield, Mappin Street, Sheffield, S1 3JD, U.K.

Abstract

$BiFeO_3$ attracts considerable attention for its rich functional properties, including room temperature coexistence of magnetic order and ferroelectricity and more recently, the discovery of conduction pathways along ferroelectric domain walls. Here, insights into the defect chemistry and electrical properties of $BiFeO_3$ are obtained by *in situ* measurements of electrical conductivity, σ, and Seebeck coefficient, α, of undoped, cation-stoichiometric $BiFeO_3$ and acceptor-doped $Bi_{1-x}Ca_xFeO_{3-\delta}$ ceramics as a function of temperature and oxygen partial pressure pO_2. $Bi_{1-x}Ca_xFeO_{3-\delta}$ exhibits *p*-type conduction; the dependencies of σ and α on pO_2 show that Ca dopants are compensated mainly by oxygen vacancies. By contrast, undoped $BiFeO_3$ shows a simultaneous increase of σ and α with increasing pO_2, indicating intrinsic behavior with electrons and holes as the main defect species in almost equal concentrations. The pO_2-dependency of σ and α cannot be described by a single point defect model but instead, is quantitatively described by a combination of intrinsic and acceptor-doped characteristics attributable to parallel conduction pathways through undoped grains and defect-containing domain walls; both contribute to the total charge transport in $BiFeO_3$. Based on this model,

we discuss the charge transport mechanism and carrier mobilities of $BiFeO_3$ and show that several previous experimental findings can readily be explained within the proposed model.

Introduction

Bismuth iron oxide, $BiFeO_3$, presents multiferroic properties at room temperature since it exhibits both G-type antiferromagnetic order with a long-periodicity spiral (T_N ~367 ºC) and ferroelectricity (T_C ~827 ºC). Consequently, it has been considered as a promising multiferroic material for potential applications in which coupling between magnetic and electrical order are involved. The processing, electrical/electromechanical properties, basic physics and device application(s) have been thoroughly summarised by Catalan and Scott [1] and Rojac *et al.*[2].

However, the defect chemistry of $BiFeO_3$ has been addressed only theoretically [3-7] and no systematic studies of its electrical conductivity, σ, and thermopower/Seebeck coefficient, α, as function of oxygen partial pressure, pO_2, are found in the literature; this may be due to the notorious difficulty of obtaining phase-pure bulk $BiFeO_3$ ceramics with low leakage currents. As far as the authors are aware, there exist only three data sets of σ *vs.* pO_2 in the temperature range 600 to 700 ºC, together with oxygen permeation characteristics, of $Bi_{1-x}Sr_xFeO_3$ ceramics [8] which show that $BiFeO_3$ is a *p*-type semiconductor in the pO_2 range ~10^{-5} to ~10^{-2} atm. In addition, σ and α *vs* pO_2 for overall-isovalent ($Bi_{0.5}K_{0.5}TiO_3$)-doped $BiFeO_3$ ceramics in the temperature range 650 to 700 ºC [9] show that conduction changes from *n*-type to *p*-type on increasing pO_2 from ~10^{-6} to 1 atm.

Recently, there has been rising awareness that some functional properties of $BiFeO_3$ may be related to its defect structure. In particular, oxygen vacancies are suggested to be the cause of unwanted leakage currents in $BiFeO_3$ [10-12]. Defect-induced functionality including electrochromic behaviour is explained by the electrical activation of oxygen vacancy complexes [13] and tuning of domain-wall conduction by annealing in controlled pO_2 [13, 14]. In order to further explore and understand the properties of $BiFeO_3$, it is desirable to assess and investigate its defect structure *in situ*. We report here an extensive experimental study of the defect structure of $BiFeO_3$ by a combination of electrical conductivity and Seebeck effect measurements as a function of pO_2 on ceramics prepared by solid state reaction.

Experimental

Ca-doped $BiFeO_3$, $Bi_{1-x}Ca_xFeO_{3-\delta}$, with compositions x = 0.01, 0.03 and 0.05 was prepared by solid state reaction as reported previously [15], using powders of Bi_2O_3 (99.99% pure, Acros Chemicals), $CaCO_3$ (99% pure, Sigma-Aldrich), and Fe_2O_3 (99% pure, Sigma-Aldrich). These were mixed in an agate mortar and pestle using acetone, pressed into pellets, heated at 850 °C for 20 min, ground, repressed, fired again at 850 °C for 20 min, ground, repressed isostatically at 200 MPa, given a final firing at ~860−945 °C for 2 h in air, and then cooled slowly. The final density of the pellets ranged from ~83 % to 95 % with increasing x.

Nominally undoped $BiFeO_3$ was prepared by mixing commercial Bi_2O_3 (99.9% pure, Sigma–Aldrich) and Fe_2O_3 (99% pure, Sigma–Aldrich) powders in an agate mortar and pestle using ethanol. Then, the powder was heated at 800 ºC for 30 min, hand-milled, compacted in a 6.35 mm die at a uniaxial pressure of 930 MPa and the resulting green pellets heated at 850 ºC for 1 min in air and then cooled slowly. The final density of the pellets was ~83 %.

The phases present were analyzed by X-Ray Powder Diffraction (XRD) using either a Stoe StadiP Diffractometer or a Panalytical X'Pert Pro diffractometer. The patterns of all samples closely resembled that of rhombohedral $BiFeO_3$ but showed that undoped $BiFeO_3$ contained a small amount of $Bi_{25}FeO_{39}$ and $Bi_2Fe_4O_9$ whereas Ca-doped $BiFeO_3$ showed no evidence of secondary phases.

For electrical property measurements, samples were mounted in a ProboStat measurement cell (NorECs, Norway), flushed with dry Ar/O_2 mixture (bubbling through P_2O_5; pH_2O ~30 ppm) of known oxygen partial pressure, pO_2 [16]. The lower limit of pO_2 investigated here (10^{-5} atm < pO_2 < 1 atm) was restricted by spurious oxygen present in the undiluted Ar. *dc* conductivity in the van der Pauw geometry and Seebeck coefficient of the $Bi_{1-x}Ca_xFeO_{3-\delta}$ samples were measured simultaneously as a function of pO_2, using a custom-made assembly described elsewhere in detail [17]. The voltage/current point contacts for the van der Pauw resistivity measurement were made of solid Pt wires, spring-loaded to the rim of the pellets. The resistivity of nominally-undoped $BiFeO_3$ was too high to measure using the same setup and, therefore, its Seebeck coefficient and impedance were measured separately. For the impedance measurements, pellets were coated with Ag electrodes made from Ag paint that was hardened by heating to 650 ºC. A Novocontrol Alpha-A (connected to a Novocontrol Pot/Gal electrochemical interface) impedance analyser was used over the frequency range 100 mHz to 10 MHz, with an *ac* measuring voltage of 100 mV, over the temperature range ~20 °C to 650 °C. The conductivity during all measurements was monitored *vs.* time at each new set of

conditions to ensure that equilibrium was achieved before taking a measurement. The oxygen partial pressure was varied in random order to assure reproducibility and consistency.

Results and Discussion

First, we show the properties of $Bi_{1-x}Ca_xFeO_{3-\delta}$ since it follows textbook behaviour for the dependence of σ and α on pO_2; second, we present and discuss the properties of undoped, cation-stoichiometric $BiFeO_3$, which exhibits more complex behaviour.

$Bi_{1-x}Ca_xFeO_{3-\delta}$

Figure 1 (a)–(f) shows conductivity and Seebeck coefficient data against pO_2 for the $Bi_{1-x}Ca_xFeO_{3-\delta}$ samples. The conductivity increases with increasing pO_2, following approximately the relation: $\sigma \propto {pO_2}^{1/4}$. The Seebeck coefficient decreases linearly with increasing $\log pO_2$. At constant pO_2, both the Seebeck coefficient and electrical conductivity are almost temperature independent but vary somewhat with the substitution level, x, Figure 1S.

On substituting Bi^{3+} with Ca^{2+} ions, point defects with an effective negative charge, Ca'_{Bi} are created. In order to preserve overall charge neutrality, these defects are balanced by defects of effective positive charge which are likely to be either electron holes or oxygen vacancies. Using Kröger-Vink notation [18] these two possible substitutions can be written as:

$$\frac{1}{4}O_2(g) + \frac{1}{2}Fe_2O_3 + CaO \leftrightarrows Ca'_{Bi} + h^{\bullet} + 3O_O^x + Fe_{Fe}^x \quad (1)$$

$$\frac{1}{2}Fe_2O_3 + CaO \leftrightarrows Ca'_{Bi} + \frac{1}{2}v_O^{\bullet\bullet} + \frac{5}{2}O_O^x + Fe_{Fe}^x \quad (1')$$

An alternative charge compensation possibility involving creation of interstitial Ca ions, $Ca_i^{\bullet\bullet}$, is considered unlikely in the perovskite structure of $BiFeO_3$.

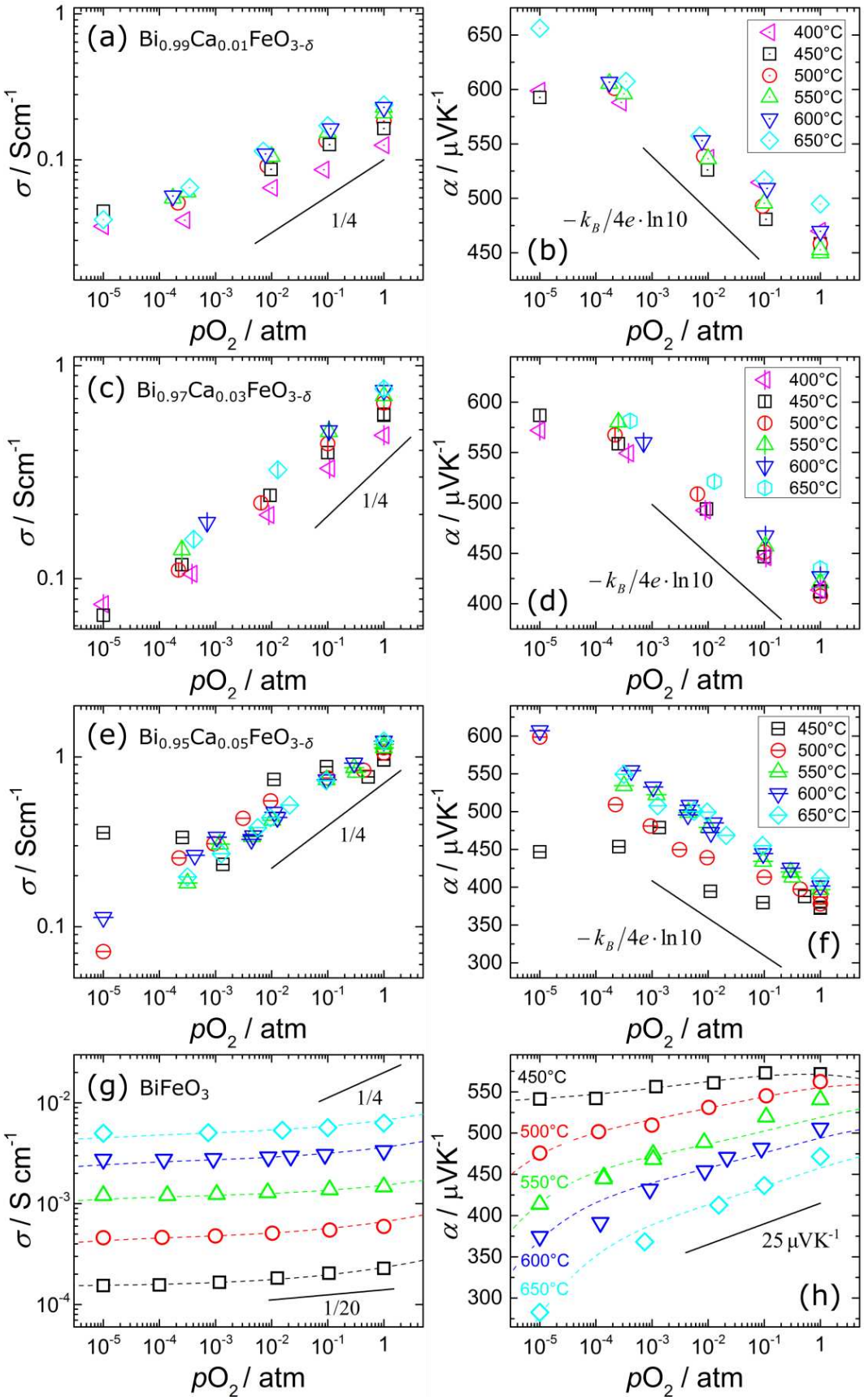

Figure 1. The electrical conductivity σ (left panels) and Seebeck coefficient α (right panels) of $Bi_{1-x}Ca_xFeO_{3-\delta}$ against pO_2 at different temperatures. **(a) – (f)** show data for Ca-doped samples with x = 0.01, 0.03, and 0.05. **(g)** and **(h)** show data for nominally undoped $BiFeO_3$. Solid lines are for ease of comparison, and dashed lines are the best fit to the model described by equations (12) and (13).

In order to account for any dependence of conductivity on pO_2, it is usually assumed that oxygen vacancies, $v_O^{\bullet\bullet}$, are required, leading to an equilibrium between $v_O^{\bullet\bullet}$ and electron holes, $h^{\bullet}$, that can be described by the defect chemical reaction:

$$v_O^{\bullet\bullet} + \frac{1}{2}O_2(g) \leftrightarrows O_O^x + 2h^{\bullet} \tag{2}$$

with the corresponding mass action law given by:

$$K_{Ox} = \frac{[O_O^x][h^{\bullet}]^2}{[v_O^{\bullet\bullet}]\sqrt{pO_2}} = \frac{(3-\delta)p^2}{\delta\sqrt{pO_2}} \tag{3}$$

where K_{Ox} is an equilibrium coefficient for the oxidation reaction (2), $p = [h^{\bullet}]$, $[O_O^x] = (3-\delta)$ *i.e.* the oxygen content in the formula $Bi_{1-x}Ca_xFeO_{3-\delta}$, $\delta = [v_O^{\bullet\bullet}]$ and pO_2 is the oxygen partial pressure. The overall charge neutrality of the sample can therefore be expressed as

$$\left[Ca_{Bi}^{/}\right] = 2[v_O^{\bullet\bullet}] + p \tag{4}.$$

In the case that $p \ll [v_O^{\bullet\bullet}]$, *i.e.* $\left[Ca_{Bi}^{/}\right] = 2[v_O^{\bullet\bullet}]$, Eq. (3) reduces to $K_{Ox} = \left(3 - [Ca_{Bi}^{/}]\right)p^2/[Ca_{Bi}^{/}]\sqrt{pO_2}$, so that the hole concentration is $p \propto {pO_2}^{1/4}$. Assuming that the mobility of holes, μ_p, is independent of their concentration, the partial electronic conductivity is also proportional to ${pO_2}^{1/4}$. The experimentally-observed ${pO_2}^{1/4}$ dependency of the total conductivity of $Bi_{1-x}Ca_xFeO_{3-\delta}$ indicates, therefore, that Ca-acceptor doping is indeed charge compensated by the formation of oxygen vacancies.

The Seebeck coefficient, α, of a non-degenerate semiconductor with electron hole-type charge carriers is often expressed as

$$\alpha = \frac{k_B}{e}\ln\frac{N_V}{p} + A_p \tag{5}$$

where N_V is the effective density of states and e is the electron charge. The energy transport term, A_p is assumed to be on the order of 20 μVK^{-1} and, therefore, commonly neglected, in particular with respect to large values of α such as reported here [19]. From Figure 1, $p \propto {pO_2}^{1/4}$ and the Seebeck coefficient is then given by: $\alpha \propto -k_B/4e \cdot \ln 10 \cdot \log pO_2$, in good agreement with the linear dependence of α on $\log pO_2$

observed for all $Bi_{1-x}Ca_xFeO_{3-\delta}$ compositions in the investigated temperature range, Figure 1. At constant pO_2, the transport coefficients do not vary significantly with temperature, Figure 1S, indicating that the hole concentration and the carrier mobility do not change significantly in the investigated temperature range.

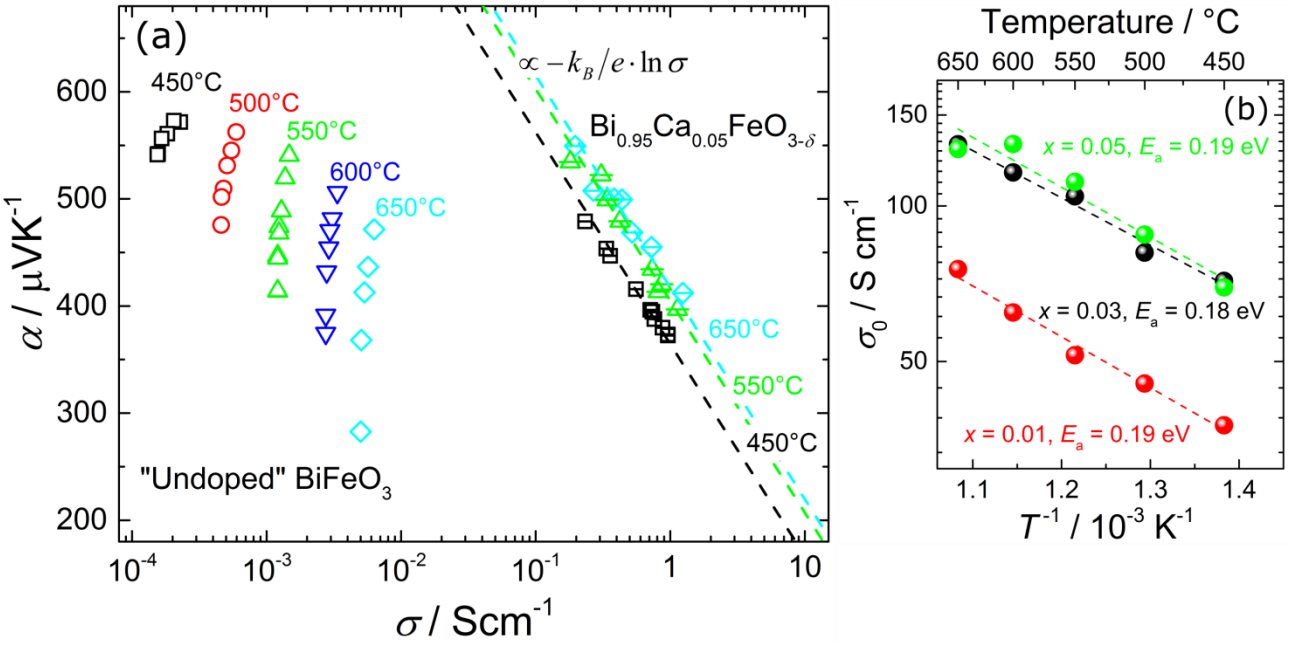

Figure 2. (a) Jonker plot of $Bi_{1-x}Ca_xFeO_{3-\delta}$. For clarity, we only show data for $x = 0$ and 0.05 at selected temperatures. Dashed lines are calculated for a non-degenerate semiconductor, $\alpha \propto -k_B/e \ln\sigma$ **(b)** The extrapolated intercept $\sigma_0 = \sigma(\alpha = 0)$ for the doped samples exhibits an activated temperature dependence with an activation energy of 0.19 eV, independent of dopant concentration x.

On further analysing together the conductivity and Seebeck data by substituting the relation $\sigma = e\mu_p p$ into equation (5) and plotting α (on linear scale) *vs.* log σ, (also referred as a Jonker plot [20]), the data for an extrinsic, *i.e.* doped, semiconductor should exhibit linear behaviour with a slope $-k_B/e \cdot \ln 10 \approx 198\ \mu VK^{-1}$, independent of the specific pO_2 at which α and σ are measured. $Bi_{1-x}Ca_xFeO_{3-\delta}$ indeed follows this relationship, Figure 2, with slight offsets between different samples, probably related to microstructural differences. Extrapolation to $\alpha = 0$ yields the product of valence band density of states, N_V, and charge carrier mobility [21]. We assume that the temperature dependence of N_V is small compared to the variation of carrier mobility with T. From the extrapolated values in Figure 2 (a), we thus obtain for $\mu_p(T)$ an activated behaviour with an activation energy of 0.19 eV, independent of Ca-dopant concentration, as shown in Figure 2 (b).

We have thus demonstrated the usefulness of simultaneous *in situ* measurements of the electrical conductivity and Seebeck coefficient under controlled pO_2 to analyse the defect structure of Ca-doped $BiFeO_3$. In particular, we have confirmed with *in situ* defect chemical measurements [22, 23] the earlier findings that acceptor-doped $BiFeO_3$ is charge-compensated by oxygen vacancies.

Undoped $BiFeO_3$

The transport properties of nominally undoped $BiFeO_3$, Figure 1 (g,h), exhibit an interesting behaviour and are very different from those of $Bi_{1-x}Ca_xFeO_{3-\delta}$. Thus, σ is nearly independent of pO_2, although critically, it increases somewhat on increasing pO_2. We note that previous σ *vs* pO_2 measurements on $BiFeO_3$ prepared by mechanosynthesis and sintered either by SPS or conventionally [24] exhibit similar dependence of σ on pO_2, Figure 2S. The behaviour is thus independent of the method and conditions in which $BiFeO_3$ is synthesised and sintered as well as the presence of small amounts of $Bi_{25}FeO_{39}$ and $Bi_2Fe_4O_9$ as secondary phases. In addition, α increases with increasing pO_2, in particular at higher temperatures. The difference to the Ca-doped samples is also obvious in the Jonker-plot, Figure 2: in "undoped" $BiFeO_3$, α decreases on decreasing log σ, whereas, in Ca-doped $BiFeO_3$, α decreases linearly on increasing log σ. Thus, the behaviour of Ca-doped $BiFeO_3$ is typical of many materials, in which the Seebeck coefficient decreases and electrical conductivity increases with increasing carrier concentration, so that α and σ vary inversely with pO_2. For this reason, the simultaneous increase of both σ and α with pO_2 observed here for undoped $BiFeO_3$, is surprising.

The unique behaviour reported here for undoped $BiFeO_3$ is further emphasised on comparing our data with those reported earlier for undoped, isovalent-doped and acceptor-doped $BiFeO_3$, Figure 3. Thus, the conductivity reported by Brinkman *et al.* [8] for nominally undoped $BiFeO_3$ increases linearly with pO_2, with similar values to those measured by us on $Bi_{0.99}Ca_{0.01}FeO_{3-\delta}$. One may speculate that the defect structure of their samples is dominated by Bi-vacancies, created during synthesis, caused by the high volatility of Bi_2O_3 [25], which leads to effectively acceptor-doped samples.

For overall-isovalent ($Bi_{0.5}K_{0.5}TiO_3$)-doped $BiFeO_3$, the conductivity passes through a minimum at ~10^{-2} atm on increasing pO_2 and, therefore, the conduction mechanism changes from *n*-type to *p*-type in a narrow pO_2 range; in the *n*-type region, $\sigma \propto {pO_2}^{-1/4}$ whereas, in the *p*-type region $\sigma \propto {pO_2}^{+1/4}$. This is

further confirmed by a change of sign of the Seebeck coefficient, from negative to positive values [9]. The point defect model proposed to account for such behaviour [9] involves the presence of both bismuth and oxygen vacancies, $v_{Bi}^{'''}$ and $v_{O}^{\bullet\bullet}$, related to the volatility of Bi_2O_3. Thus, in overall-isovalent ($Bi_{0.5}K_{0.5}TiO_3$)-doped $BiFeO_3$, ionic species dominate the defect structure, although electronic minority species are the majority charge carriers; plots of log σ *vs* log pO_2 around the *p*-*n*-transition exhibit a V-shape with "ideal" slopes of +¼ and –¼ in the *p*- and *n*-regions, respectively; the pO_2-range of the transition is small, independently of material specific parameters and in the absence of an electrolytic domain associated with oxide ion conduction.

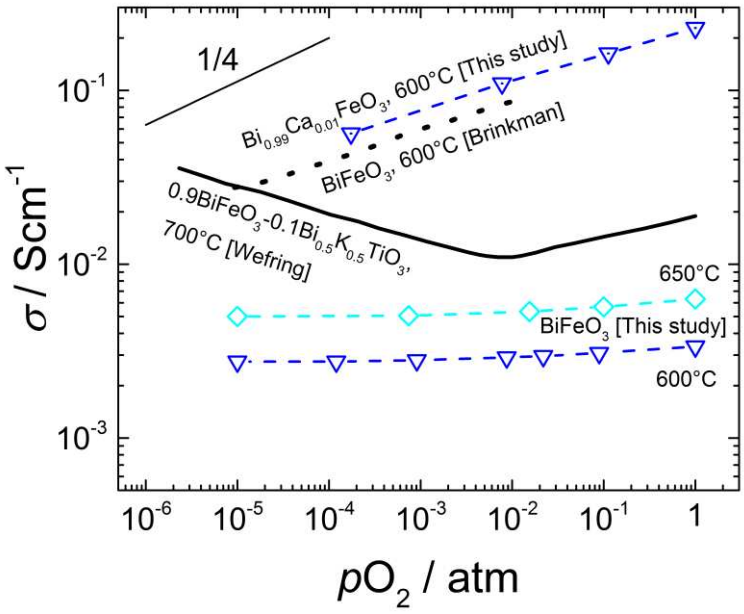

Figure 3. Comparison of the conductivity reported here with data from the literature [8, 9].

Our measurements on nominally undoped $BiFeO_3$ are significantly less sensitive to pO_2; the conductivity does not pass through a minimum in the entire pO_2 range investigated and the Seebeck coefficient remains positive. A pO_2-independent behaviour conductivity is commonly an indication of ionic conduction. Oxide Ion conductors with blocking electrodes show in the impedance spectra an inclined Warburg spike at low frequency associated with charge transfer impedances at the sample-electrode-air interface. This is not the case for undoped $BiFeO_3$ reported here since impedance measurements at different temperatures and atmospheres, Figure 3S, show no evidence of such feature at low frequency. Consequently, we discard ionic conductivity as a possible origin of the pO_2-independent conductivity of undoped $BiFeO_3$.

An alternative explanation is that materials in which intrinsic ionisation of electrons across the band gap controls their electrical properties also exhibit pO_2-independece of both σ and α. However, intrinsic ionisation of electrons cannot solely explain the electrical properties reported here since both σ and α show some dependency on pO_2. We believe that the majority of defects are electronic in nature and the sample should be close to a transition from *p*- to *n*-type behaviour.

We have investigated two possible defect models to account quantitatively for the behaviour of σ and α, as discussed next.

Initial defect model

We first qualitatively assess a defect model founded on intrinsic ionisation of electrons across the band gap, which accounts for some of our observations on undoped $BiFeO_3$. The transport coefficients indicate proximity to a transition from *p*- to *n*-type behaviour, and therefore, both electrons and holes have to be considered in the charge neutrality expression:

$$n = 2[\mathrm{v}_\mathrm{O}^{\bullet\bullet}] + p \tag{6}$$

where $n = [e']$.

The weak dependency of σ on pO_2 further indicates that the sample is close to intrinsic behaviour, *i.e.* equal concentration of electrons and holes, $n = p$. As the transport coefficients still show some dependency on pO_2, the electron and hole charge carrier concentration can vary depending on the oxygen stoichiometry, equation (2), which, thereby, perturbs the intrinsic balance of electrons and holes.

The concentrations of holes and electrons are interrelated via the charge disproportionation reaction:

$$\mathrm{nil} \leftrightarrows h^{\bullet} + e' \tag{7}$$

with the equilibrium constant $K_D = n \cdot p$. Equation (7) corresponds to thermal excitation of an electron-hole pair across the band gap of the material.

The charge neutrality condition for undoped $BiFeO_{3-\delta}$ can thus be written as:

$$\frac{K_D}{p} = 2[\mathrm{v}_\mathrm{O}^{\bullet\bullet}] + p \tag{8}.$$

Combining Equations (3) and (8), the hole concentration can be calculated as a function of pO_2 by solving:

$$p + \frac{6p^2}{p^2 + K_{\mathrm{Ox}}\sqrt{p\mathrm{O}_2}} - \frac{K_{\mathrm{D}}}{p} = 0 \tag{9}$$

K_{Ox} and K_{D} are free parameters, fixed at constant temperature. Once p is determined, the concentration of the other considered species, *i.e.* electrons and oxygen vacancies, can be calculated easily using equation (8). The total conductivity is given by $\sigma_{\mathrm{Tot}} = \sigma_p + \sigma_n = \mu_p ep + \mu_n en$, where μ_p and μ_n are the mobility of holes and electrons, respectively. The total Seebeck coefficient is related to the sum of the individual Seebeck coefficients of holes and electrons, α_p and α_n, calculated using equation (5), and weighted by their contribution to the total conductivity: $\alpha_{\mathrm{Tot}} = (\sigma_p\alpha_p + \sigma_n\alpha_n)/\sigma_{\mathrm{Tot}}$. Blue lines in Figure 4 show the defect concentration, conductivity, and Seebeck coefficient *vs.* $p\mathrm{O}_2$ for selected parameters of K_{Ox}, K_{D} and μ_p/μ_n. To simulate the effect of an increase in temperature, the equilibrium constant for charge disproportionation, K_{D}, is increased.

We now discuss the qualitative $p\mathrm{O}_2$ dependence of transport properties for this model, and compare it with our experimental data. At high $p\mathrm{O}_2$, the concentration of oxygen vacancies is small compared to that of electronic defects, so that $n = p$ in equation (6). On decreasing $p\mathrm{O}_2$, oxygen vacancies are formed, the concentration of holes decreases, *i.e.* reaction (2) is shifted to the left, and, consequently, the concentration of electrons increases. If the mobility of holes is higher than that of electrons, $\mu_p > \mu_n$, the total conductivity decreases somewhat first on decreasing $p\mathrm{O}_2$ and then increases. On increasing the temperature, σ increases but the overall behaviour remains similar. We note that the functional dependency of σ on $p\mathrm{O}_2$ and the span in $p\mathrm{O}_2$ before σ reaches its minimum are determined by the mobility ratio and the value of K_{Ox}, *i.e.* parameters specific to the material, thereby allowing the flat $p\mathrm{O}_2$-dependency observed experimentally. This contrasts with a defect structure dominated by ionic defects, where the $p\mathrm{O}_2$-dependency and the width in $p\mathrm{O}_2$ of the *p*-*n*-transition is essentially independent of the material. Thus, the model agrees qualitatively with the experimentally-observed conductivity of undoped $\mathrm{BiFeO}_{3-\delta}$: dependence of σ on $p\mathrm{O}_2$ is almost flat, but shows a strong increase with temperature. By contrast, α initially decreases somewhat on decreasing $p\mathrm{O}_2$ and then decreases almost linearly. On increasing the temperature, α decreases, the slope in the linear behaviour increases and even negative values (*n*-type behaviour) are expected at the lowest $p\mathrm{O}_2$. We note that the temperature dependence of K_{Ox}, μ_p, and μ_n has been neglected since, as discussed earlier, these appear to be small compared to that of K_{D}.

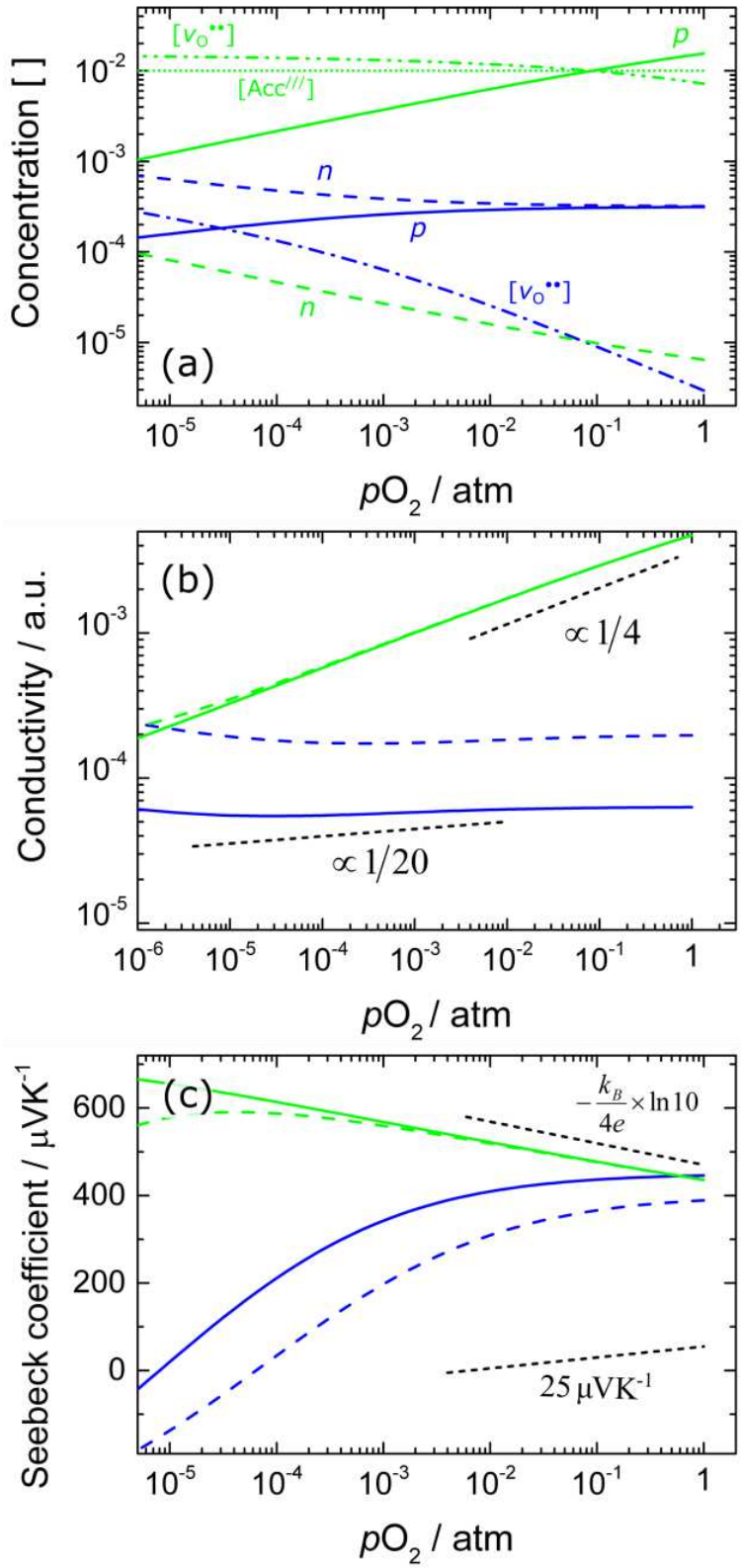

Figure 4. Qualitative model of the defect chemistry of undoped (blue line) and acceptor-doped (green line) $BiFeO_3$ ceramics. **(a)** Defect concentration, **(b)** conductivity and **(c)** Seebeck coefficient against pO_2. All coefficients in (b) and (c) have been calculated using: $K_{Ox} = 0.1$ and

$\mu_p/\mu_n = 3$. An increase of temperature is simulated by a tenfold increase of K_D from 10^{-7} (solid line) to 10^{-6} (dashed line).

This model can be easily extended to acceptor-doped compositions, by adding the specific acceptor concentration on the left side of equation (6):

$$z\left[\mathrm{Acc}^{z/}\right] + n = 2[\mathrm{v}_\mathrm{O}^{\bullet\bullet}] + p \quad (10).$$

Here, z indicates the effective charge of the acceptor, *e.g.* $z = 1$ for Ca-dopants, $\mathrm{Ca}_\mathrm{Bi}^{/}$, or $z = 3$ for Bi vacancies, $\mathrm{v}_\mathrm{Bi}^{///}$. Combining equations (3), (7), and (10) then provides a general expression for both the doped and undoped cases:

$$p + \frac{6p^2}{p^2 + K_\mathrm{Ox}\sqrt{p\mathrm{O}_2}} - \frac{K_\mathrm{D}}{p} - z\left[\mathrm{Acc}^{z/}\right] = 0 \quad (11).$$

If the acceptor concentration is larger than that of thermally excited charge carriers, this model is equivalent to the one presented earlier for $Bi_{1-x}Ca_xFeO_{3-\delta}$ (equations (1)–(4)). To illustrate this, we calculate the transport coefficients for a sample with an acceptor concentration of 0.01 and the same values of K_Ox, K_D, and μ_p/μ_n as used for undoped $BiFeO_{3-\delta}$: In this case, $\sigma \propto p(\mathrm{O}_2)^{+1/4}$ and $\alpha \propto -k_B/4e \cdot \ln 10 \cdot \log p(\mathrm{O}_2)$; neither σ nor α vary significantly with temperature, in good agreement with the experimental observation.

This initial defect model can qualitatively account for the experimentally-observed dependences of σ and α on temperature and $p\mathrm{O}_2$ for both doped and undoped $BiFeO_3$. However, all attempts to quantitatively fit the data were unsuccessful since the predicted variation of the Seebeck coefficient with $p\mathrm{O}_2$ is much larger than observed experimentally. Different defect chemical models, which contain point defects such as metal vacancies or Frenkel defects, were also unable to fit the data for the same reason. This could be related to equation (5) of the Seebeck coefficient which may be too simple for quantitative analysis. However, since the functional dependency of α on p and $p\mathrm{O}_2$, is as expected for $Bi_{1-x}Ca_xFeO_{3-\delta}$, it is unclear why it is unable to describe the behaviour of undoped $BiFeO_{3-\delta}$.

Two region defect model

Recently, Rojac *et al.* [14] provided atomic-scale chemical and structural evidence of accumulation of bismuth vacancies at domain walls in $BiFeO_3$ and further showed that the local domain wall conductivity can be tuned on annealing $BiFeO_3$ in different pO_2 at 700 °C. These results highlight that the chemical composition –and thus the defect chemistry– of $BiFeO_3$ ceramics may not be homogeneous throughout and in particular, the bulk (grains) and domain walls may well show different electronic behaviour.

Inspired by this finding, we hypothesise that the total conductivity of nominally-undoped $BiFeO_3$ has two contributions: one from regions of effectively-undoped $BiFeO_3$, which is almost independent of pO_2, and another from regions of acceptor-doped $BiFeO_3$, with a defect structure similar to that found for $Bi_{1-x}Ca_xFeO_{3-\delta}$, *i.e.*

$$\sigma_{\mathrm{Tot}}(pO_2) = \sigma_1 + \sigma_2(pO_2) \quad (12).$$

We note that such a scenario requires that conduction through both regions should occur in parallel. Also, charge transport in both regions can itself have contributions from both electrons and holes. To test our hypothesis, we proceeded as follows:

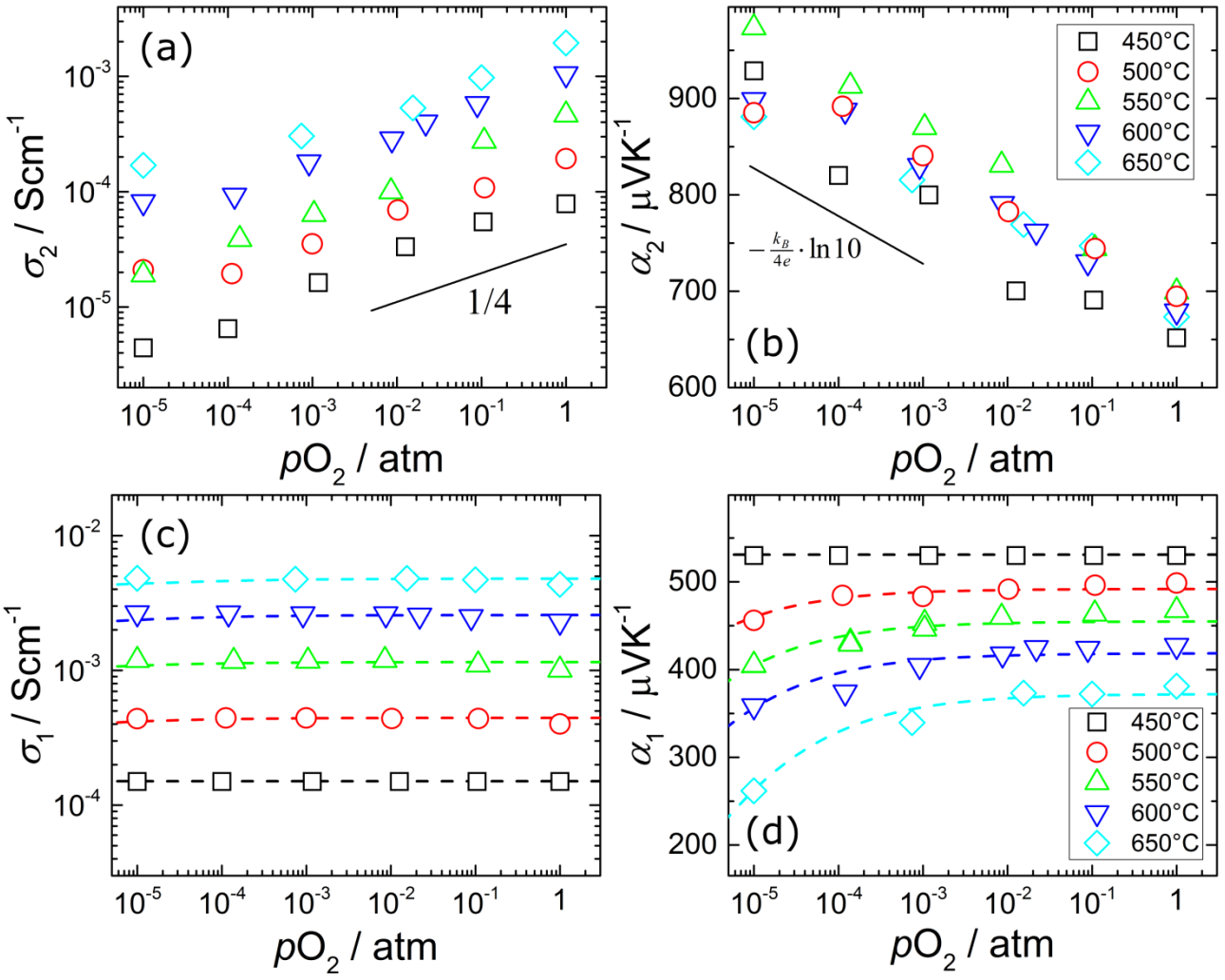

Figure 5. Transport coefficients σ and α of undoped $BiFeO_3$, assuming the two individual contributions specified in equation (12) and (13). σ_2 **(a)** and α_2 **(b)** show typical behaviour of acceptor-doped $BiFeO_3$, while σ_1 **(c)** and α_1 **(d)** correspond to undoped behaviour.

Initially, as a first approximation, we chose~~set~~ σ_1 ~~$= \sigma_{Min}(pO_2)$, *i.e.*~~close to the conductivity minimum of the pO_2 curve, for each temperature and subtracted it from σ_{Tot} to obtain $\sigma_2(pO_2)$. Then, σ_2 at high pO_2 is extrapolated to low pO_2 to refine the value of σ_1. Figure 5 (a) shows that σ_2 indeed exhibits a clear ¼-dependency on pO_2 at all temperatures, resembling the behaviour of an acceptor-doped region. This indicates therefore that our approach to separate σ_1 and σ_2 is reasonable.

As well as the conductivity, in this scenario, the Seebeck coefficient should also contain two contributions, weighted by their relative conductivity, *i.e.*

$$\alpha_{Tot}(pO_2) = \frac{\alpha_1 \cdot \sigma_1 + \alpha_2(pO_2) \cdot \sigma_2(pO_2)}{\sigma_{Tot}(pO_2)} \quad (13).$$

By adjusting α_1, α_2 can thus be calculated. At 450°C, the obtained $\alpha_2(pO_2)$ is proportional to $-k_B/4e \cdot \ln 10 \cdot \log pO_2$, which is again the fingerprint of an acceptor-doped defect structure. This result further supports our analysis.

At higher temperatures, the assumption of contribution 1 with $n = p$, in the entire pO_2-range studied, no longer holds since the tendency towards oxygen loss increases and shifts the onset of the p- to n-transition to higher pO_2 on increasing temperature (see Figures 4 (b) and (c)). Deviations from $n = p$ are more pronounced in the Seebeck coefficient, as compared to the conductivity. Therefore, we allow slight adjustments of α_1 in order to obtain sensible values for $\alpha_2(pO_2)$. Figure 5 (a)-(d) shows the deconvoluted values of σ_{Tot} and α_{Tot} for contributions 1 and 2. Summarising, σ_1 is pO_2-independent at all temperatures whereas α_1 is almost pO_2-independent at the lowest temperatures but, at the highest temperatures, α_1 first increases on increasing pO_2 and then flattens out, approaching a constant value at high pO_2. By contrast, both σ_2 and α_2 depend strongly on pO_2. α_2 appears to be temperature-independent, whereas σ_2 exhibits a large temperature-dependency with activation energy ~0.7 eV. This activation energy for σ_2 is greater than that of $Bi_{1-x}Ca_xFeO_{3-\delta}$, which indicates that charge carriers are electrostatically trapped to a larger extent. We speculate that acceptor bismuth vacancies (effectively triple charged in comparison with singly charged Ca dopants) created during sintering may account for the difference in activation energy. Another explanation of the relatively high activation energy within region 2 could be due to carrier trapping at oxygen vacancy clusters, as suggested by Farokhipoor *et al.* [26]. Similar values of mobility activation energies and spatial variations across the sample have been reported earlier [13, 27].

Next, by allowing variation of K_D, K_{Ox}, μ_p, μ_n, we simultaneously fit the conductivity and Seebeck coefficient for the undoped model, equation (9), to the derived values of σ_1 and α_1, indicated as dashed lines in Figure 5. Details of the optimization procedure are given in the supplementary information. Due to the number of independent parameters, in principle, several sets of parameter values may describe the data equally well. However, we note that – independent of the chosen starting values – the fitted parameters are self-consistent for the temperatures investigated and their values are physically meaningful, Figure 6. For example, we obtain a temperature-dependence of K_D with activation energy 1.3 eV, which is identical to the reported value of the band gap of bulk $BiFeO_3$, E_g = ~~2.5–2.8~~1.3 eV [28]. We note that band gaps of $BiFeO_3$ thin film samples are often significantly larger, E_g = 2.5-2.8 eV [4, 29, 30], which has been assigned to

changes in the orbital overlap due to substrate induced strain and stress. Further, the activation energy for the mobility of holes, 0.3 eV, is similar to our results for $Bi_{1-x}Ca_xFeO_{3-\delta}$ and in agreement with earlier reported values [27, 31-33]. The activation energy of electron mobility is higher, 0.5 eV and the mobility ratio, μ_p/μ_n decreases from ~5.5 at 450°C to ~2.7 at 650 °C.

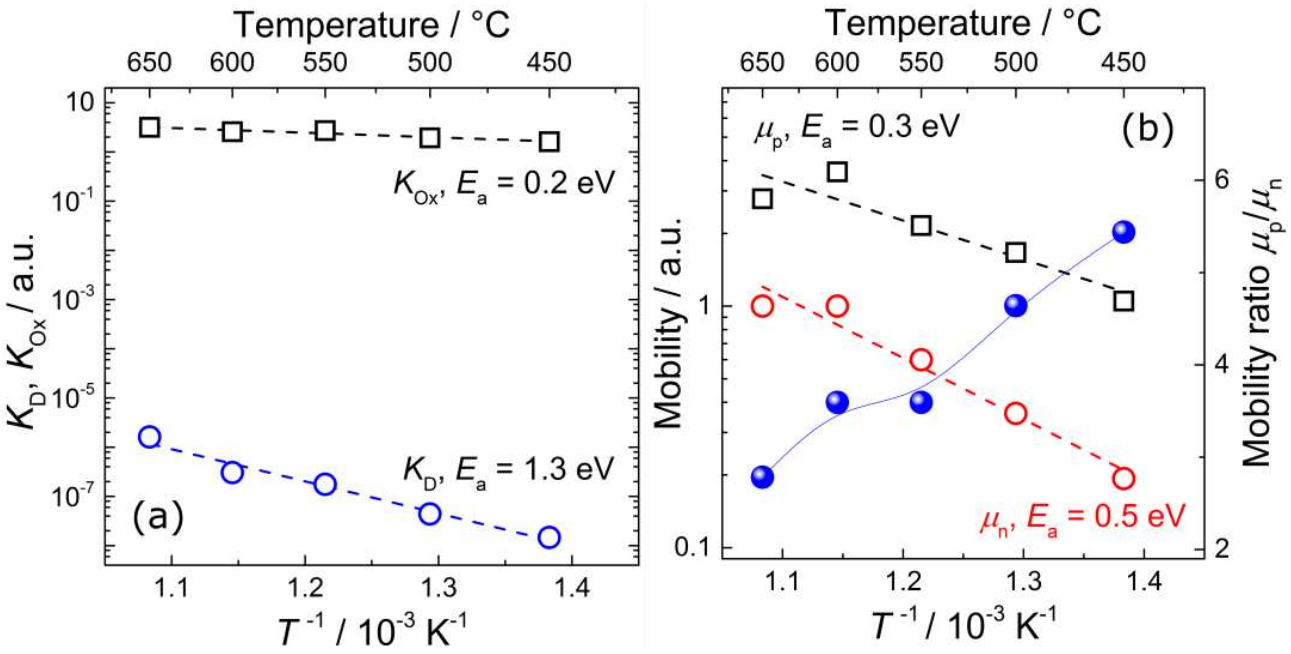

Figure 6. Optimized parameters describing the bulk properties of $BiFeO_3$. **(a)** The equilibrium constants K_{Ox} and K_D show thermally activated behaviour. **(b)** Both hole and electron mobility show an activated behaviour, with $\mu_p > \mu_n$ in the investigated temperature range. The mobility ratio μ_p/μ_n (blue filled circles) is around 4 and decreases with increasing temperature.

Using the raw data shown in Figures 1 (g) and (h), it is now possible to quantitatively describe the data of both contributions using the defect chemical model outlined above, where contribution 1 resembles virtually undoped material and contribution 2 follows the behaviour of an acceptor-doped defect structure. Figure 7 illustrates as an example how the two contributions influence the total transport coefficients at 550°C. Dashed lines in Figure 1(g) and (h) obtained by combining the calculated transport parameters of contributions 1 and 2 using equations (12) and (13) reproduce the experimental data to a high degree.

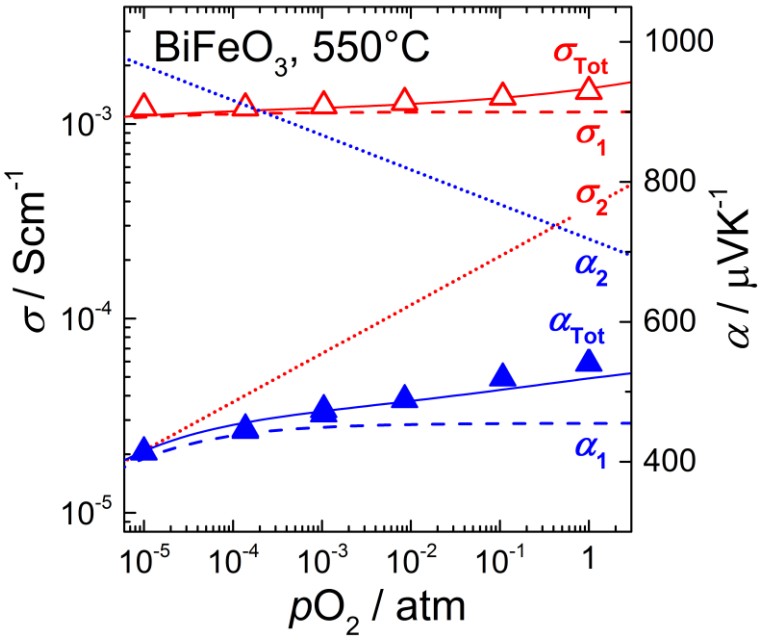

Figure 7. Deconvolution of the total transport coefficients of nominally-undoped $BiFeO_3$ into contributions 1 and 2, as explained in the text.

Using the above procedure, we have successfully disentangled the transport properties of nominally-undoped $BiFeO_3$ into two contributions, a dominant part close to intrinsic behaviour, $n = p$, and a minor contribution, which resembles our measurements on Ca-(acceptor)-doped $BiFeO_3$. So far, this treatment is purely phenomenological, and no physical interpretation was involved or necessary. To interpret these findings, we consider that agglomeration of Bi-vacancies within ferroelectric domain walls (DW), as has been reported recently by Rojac *et al.*[14], is a plausible scenario, Figure 8. The domain walls would provide a parallel rail for electrical transport, with distinctively different pO_2-dependence to that of effectively undoped $BiFeO_3$. If this is the case, the charge compensation mechanism at the domain walls suggested here, *i.e.* Bi vacancies compensated with oxygen vacancies, differs from that of Bi vacancies compensated with holes proposed by Rojac *et al.*[14], in which the DW conductivity should be pO_2-independent since the charge neutrality is given by $3\left[v_{Bi}^{'''}\right] = p$. Rojac *et al.* [14] showed that the DW conductivity could indeed be tuned with pO_2 which indicates that ionic defects are charge compensated by oxygen vacancies rather than holes, in support of our model. In addition, assuming that charge transport occurs via localized states associated with Fe, *i.e.* electrons as Fe^{2+} and holes as Fe^{4+}, our results indicate that the oxidation state of Fe at the domain walls should be equal to or slightly greater than 3+, whereas Rojac *et al.* proposed Fe^{4+}. We do, however, both agree that Fe is 3+ in the bulk.

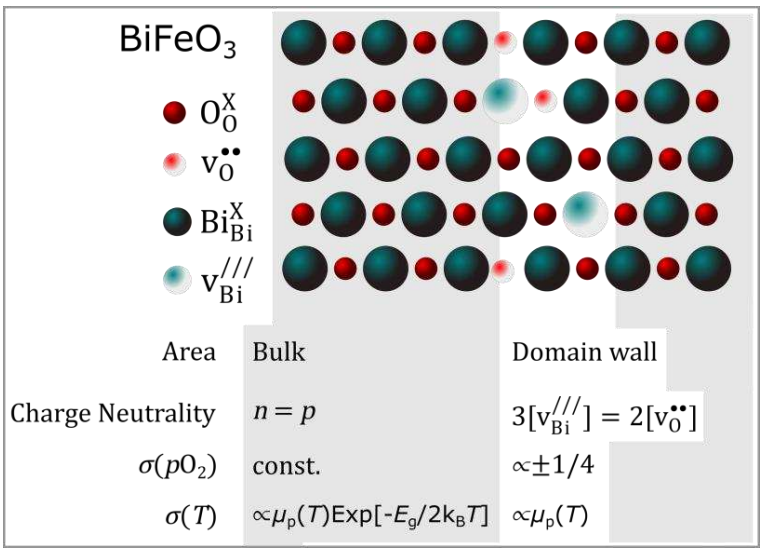

Figure 8. Schematic of the proposed two domain model to describe $BiFeO_3$. Fe atoms are omitted for clarity. The defect structure of bulk and domain walls is different, so that transport coefficients show different behaviour with temperature and pO_2.

Moreover, the formation of domain walls at locations with enriched agglomeration/accumulation of charged, ionic defects not only explains our results and those of Rojac *et al.*, but also previous findings such as pO_2 sensitivity of the DW conduction [13, 34] as well as decoupling of conductive footprints and DW position upon poling [35]. Relating DWs in ferroelectrics with an accumulation of charged defects may further provide a qualitative explanation for the low velocity of the wall movement during switching, since heavy, ionic species have to be moved [36, 37].

We note that charge transport within DWs in $BiFeO_3$ via localized hopping conduction contrasts with that observed in other ferroelectric materials such as $YbMnO_3$ and $BaTiO_3$, which show greater carrier mobility at DWs, comparable to conventional semiconductors [38, 39] and thus a delocalised charge transport. This underlines the notion that DW conduction in multiferroic materials may have several different origins and characteristics, which makes further investigation both necessary and exciting. In future, it would be interesting to investigate the spatial variation of both transport coefficients in $BiFeO_3$ at different pO_2 and temperature. Increasing the temperature or decreasing pO_2 further, may eventually lead to the peculiar situation of bulk (*n*-type) and domain walls (*p*-type) with different majority charge carriers, which may lead to interesting, new effects.

Conclusion

We have investigated the defect chemistry of high quality, polycrystalline, nominally undoped and cation stoichiometric $BiFeO_3$ and acceptor-doped $Bi_{1-x}Ca_xFeO_{3-\delta}$ ceramics by measuring both their electrical conductivity and Seebeck coefficient simultaneously at different temperatures and oxygen partial pressures. In both $BiFeO_3$ and $Bi_{1-x}Ca_xFeO_{3-\delta}$, the Seebeck coefficient is positive for all samples and experimental conditions, indicating that electron holes are the major contributor to the electronic conduction. Our analysis shows that Ca-(acceptor)-doped $BiFeO_{3-\delta}$ is charge-compensated by the formation of oxygen vacancies. Nominally undoped $BiFeO_3$ shows a clearly different behaviour, with an almost pO_2-independent conductivity and a small pO_2-dependency of the Seebeck coefficient, which is indicative of a defect structure with a small concentration of ionic defects and is close to intrinsic behaviour with equal concentrations of electrons and holes. We rationalize these observations quantitatively by visualising the sample as consisting of two regions with different composition that contribute to the total charge transport in nominally undoped $BiFeO_3$. Bi-vacancy agglomeration at domain walls and essentially, defect-free undoped bulk are discussed as a possible identification of these regions. These results demonstrate that *in situ* measurements of charge transport under well-defined experimental conditions can be a powerful tool to understand multifunctional materials. We finally show that this scenario can qualitatively explain a range of previous observations in $BiFeO_3$.

Acknowledgments

The authors are grateful to Prof. Truls Norby for discussions and helpful suggestions on the manuscript. We thank EPSRC, and the research council of Norway (Grants 219731 and 228854) for financial support. Financial support from Projects CTQ2014-52763-C2-1-R (MINECO-FEDER) and TEP-7858 (Junta Andalucía-FEDER), is also acknowledged. AP thanks VPPI-US for his current contract.

References

[1] Catalan, G. and J.F. Scott, *Physics and Applications of Bismuth Ferrite.* Advanced Materials, 2009. **21**(24): p. 2463-2485.

[2] Rojac, T., A. Bencan, B. Malic, G. Tutuncu, J.L. Jones, J.E. Daniels, and D. Damjanovic, *$BiFeO_3$ Ceramics: Processing, Electrical, and Electromechanical Properties.* Journal of the American Ceramic Society, 2014. **97**(7): p. 1993-2011.

[3] Ederer, C. and N.A. Spaldin, *Influence of strain and oxygen vacancies on the magnetoelectric properties of multiferroic bismuth ferrite.* Physical Review B, 2005. **71**(22): p. 224103.

[4] Clark, S.J. and J. Robertson, *Band gap and Schottky barrier heights of multiferroic $BiFeO_3$.* Applied Physics Letters, 2007. **90**(13): p. 132903.
[5] Paudel, T.R., S.S. Jaswal, and E.Y. Tsymbal, *Intrinsic defects in multiferroic $BiFeO_3$ and their effect on magnetism.* Physical Review B, 2012. **85**(10): p. 104409.
[6] Xu, Q., M. Sobhan, Q. Yang, F. Anariba, K. Phuong Ong, and P. Wu, *The role of Bi vacancies in the electrical conduction of $BiFeO_3$: a first-principles approach.* Dalton Transactions, 2014. **43**(28): p. 10787-10793.
[7] Shimada, T., T. Matsui, T. Xu, K. Arisue, Y. Zhang, J. Wang, and T. Kitamura, *Multiferroic nature of intrinsic point defects in $BiFeO_3$: A hybrid Hartree-Fock density functional study.* Physical Review B, 2016. **93**(17): p. 174107.
[8] Brinkman, K., T. Iijima, and H. Takamura, *The oxygen permeation characteristics of $Bi_{1-x}Sr_xFeO_3$ mixed ionic and electronic conducting ceramics.* Solid State Ionics, 2010. **181**(1–2): p. 53-58.
[9] Wefring, E.T., M.A. Einarsrud, and T. Grande, *Electrical conductivity and thermopower of $(1 - x)\ BiFeO_3 - x Bi_{0.5}K_{0.5}TiO_3$ ($x = 0.1, 0.2$) ceramics near the ferroelectric to paraelectric phase transition.* Physical Chemistry Chemical Physics, 2015. **17**(14): p. 9420-9428.
[10] Wu, J., J. Wang, D. Xiao, and J. Zhu, *Migration Kinetics of Oxygen Vacancies in Mn-Modified BiFeO3 Thin Films.* ACS Applied Materials & Interfaces, 2011. **3**(7): p. 2504-2511.
[11] Zhu, H., X. Sun, L. Kang, M. Hong, M. Liu, Z. Yu, and J. Ouyang, *Charge transport behaviors in epitaxial BiFeO3 thick films sputtered with different Ar/O2 flow ratios.* Scripta Materialia, 2016. **115**: p. 62-65.
[12] Yang, H., H. Wang, G.F. Zou, M. Jain, N.A. Suvorova, D.M. Feldmann, P.C. Dowden, R.F. DePaula, J.L. MacManus-Driscoll, A.J. Taylor, and Q.X. Jia, *Leakage mechanisms of self-assembled (BiFeO3)0.5:(Sm2O3)0.5 nanocomposite films.* Applied Physics Letters, 2008. **93**(14): p. 142904.
[13] Seidel, J., P. Maksymovych, Y. Batra, A. Katan, S.Y. Yang, Q. He, A.P. Baddorf, S.V. Kalinin, C.H. Yang, J.C. Yang, Y.H. Chu, E.K.H. Salje, H. Wormeester, M. Salmeron, and R. Ramesh, *Domain Wall Conductivity in La-Doped $BiFeO_3$.* Physical Review Letters, 2010. **105**(19): p. 197603.
[14] Rojac, T., A. Bencan, G. Drazic, N. Sakamoto, H. Ursic, B. Jancar, G. Tavcar, M. Makarovic, J. Walker, B. Malic, and D. Damjanovic, *Domain-wall conduction in ferroelectric $BiFeO_3$ controlled by accumulation of charged defects.* Nat Mater, 2017. **16**(3): p. 322-327.
[15] Masó, N. and A.R. West, *Electrical Properties of Ca-Doped $BiFeO_3$ Ceramics: From p-Type Semiconduction to Oxide-Ion Conduction.* Chemistry of Materials, 2012. **24**(11): p. 2127-2132.
[16] Norby, T., *EMF method determination of conductivity contributions from protons and other foreign ions in oxides.* Solid State Ionics, 1988. **28**: p. 1586-1591.
[17] Schrade, M., H. Fjeld, T. Norby, and T.G. Finstad, *Versatile apparatus for thermoelectric characterization of oxides at high temperatures.* Review of Scientific Instruments, 2014. **85**(10): p. 103906.
[18] Kröger, F.A. and H.J. Vink, *Relations between the Concentrations of Imperfections in Crystalline Solids.* Solid State Physics, 1956. **3**: p. 307-435.
[19] Mizusaki, J., T. Sasamoto, W.R. Cannon, and H.K. Bowen, *Electronic Conductivity, Seebeck Coefficient, and Defect Structure of $LaFeO_3$.* Journal of the American Ceramic Society, 1982. **65**(8): p. 363-368.
[20] Jonker, G.H., *The application of combined conductivity and Seebeck-effect plots for the analysis of semiconductor properties.* Philips Res. Rep., 1968. **23**(2): p. 131-8.
[21] Zhu, Q., E.M. Hopper, B.J. Ingram, and T.O. Mason, *Combined Jonker and Ioffe Analysis of Oxide Conductors and Semiconductors.* Journal of the American Ceramic Society, 2011. **94**(1): p. 187-193.

[22] Yang, C.-H., D. Kan, I. Takeuchi, V. Nagarajan, and J. Seidel, *Doping $BiFeO_3$: approaches and enhanced functionality.* Physical Chemistry Chemical Physics, 2012. **14**(46): p. 15953-15962.

[23] Schiemer, J.A., R.L. Withers, Y. Liu, and M.A. Carpenter, *Ca-Doping of $BiFeO_3$: The Role of Strain in Determining Coupling between Ferroelectric Displacements, Magnetic Moments, Octahedral Tilting, and Oxygen-Vacancy Ordering.* Chemistry of Materials, 2013. **25**(21): p. 4436-4446.

[24] Perejón, A., N. Masó, A.R. West, P.E. Sánchez-Jiménez, R. Poyato, J.M. Criado, and L.A. Pérez-Maqueda, *Electrical Properties of Stoichiometric $BiFeO_3$ Prepared by Mechanosynthesis with Either Conventional or Spark Plasma Sintering.* Journal of the American Ceramic Society, 2013. **96**(4): p. 1220-1227.

[25] Bogle, K.A., J. Cheung, Y.-L. Chen, S.-C. Liao, C.-H. Lai, Y.-H. Chu, J.M. Gregg, S.B. Ogale, and N. Valanoor, *Epitaxial Magnetic Oxide Nanocrystals Via Phase Decomposition of Bismuth Perovskite Precursors.* Advanced Functional Materials, 2012. **22**(24): p. 5224-5230.

[26] Farokhipoor, S. and B. Noheda, *Conduction through 71° Domain Walls in $BiFeO_3$ Thin Films.* Physical Review Letters, 2011. **107**(12): p. 127601.

[27] Seidel, J., M. Trassin, Y. Zhang, P. Maksymovych, T. Uhlig, P. Milde, D. Köhler, A.P. Baddorf, S.V. Kalinin, L.M. Eng, X. Pan, and R. Ramesh, *Electronic Properties of Isosymmetric Phase Boundaries in Highly Strained Ca-Doped $BiFeO_3$.* Advanced Materials, 2014. **26**(25): p. 4376-4380.

[28] Higuchi, T., Y.-S. Liu, P. Yao, P.-A. Glans, J. Guo, C. Chang, Z. Wu, W. Sakamoto, N. Itoh, T. Shimura, T. Yogo, and T. Hattori, *Electronic structure of multiferroic ${\text{BiFeO}}_{3}$ by resonant soft x-ray emission spectroscopy.* Physical Review B, 2008. **78**(8): p. 085106.

[29] Palai, R., R.S. Katiyar, H. Schmid, P. Tissot, S.J. Clark, J. Robertson, S.A.T. Redfern, G. Catalan, and J.F. Scott, *β phase and $\gamma-\beta$ metal-insulator transition in multiferroic $BiFeO_3$.* Physical Review B, 2008. **77**(1): p. 014110.

[30] Kanai, T., S.-i. Ohkoshi, and K. Hashimoto, *Magnetic, electric, and optical functionalities of (PLZT)x(BiFeO3)1−x ferroelectric–ferromagnetic thin films.* Journal of Physics and Chemistry of Solids, 2003. **64**(3): p. 391-397.

[31] Ke, Q., X. Lou, Y. Wang, and J. Wang, *Oxygen-vacancy-related relaxation and scaling behaviors of $Bi_{0.9}La_{0.1}Fe_{0.98}Mg_{0.02}O_3$ ferroelectric thin films.* Physical Review B, 2010. **82**(2): p. 024102.

[32] Lim, J.S., J.H. Lee, A. Ikeda-Ohno, T. Ohkochi, K.-S. Kim, J. Seidel, and C.-H. Yang, *Electric-field-induced insulator to Coulomb glass transition via oxygen-vacancy migration in Ca-doped $BiFeO_3$.* Physical Review B, 2016. **94**(3): p. 035123.

[33] Hunpratub, S., P. Thongbai, T. Yamwong, R. Yimnirun, and S. Maensiri, *Dielectric relaxations and dielectric response in multiferroic $BiFeO_3$ ceramics.* Applied Physics Letters, 2009. **94**(6): p. 062904.

[34] Daumont, C.J.M., S. Farokhipoor, A. Ferri, J.C. Wojdeł, J. Íñiguez, B.J. Kooi, and B. Noheda, *Tuning the atomic and domain structure of epitaxial films of multiferroic $BiFeO_3$.* Physical Review B, 2010. **81**(14): p. 144115.

[35] Stolichnov, I., M. Iwanowska, E. Colla, B. Ziegler, I. Gaponenko, P. Paruch, M. Huijben, G. Rijnders, and N. Setter, *Persistent conductive footprints of 109° domain walls in bismuth ferrite films.* Applied Physics Letters, 2014. **104**(13): p. 132902.

[36] McGilly, L.J., L. Feigl, T. Sluka, P. Yudin, A.K. Tagantsev, and N. Setter, *Velocity Control of 180° Domain Walls in Ferroelectric Thin Films by Electrode Modification.* Nano Letters, 2016. **16**(1): p. 68-73.

[37] McGilly, L.J., YudinP, FeiglL, A.K. Tagantsev, and SetterN, *Controlling domain wall motion in ferroelectric thin films.* Nat Nano, 2015. **10**(2): p. 145-150.

[38] Sluka, T., A.K. Tagantsev, P. Bednyakov, and N. Setter, *Free-electron gas at charged domain walls in insulating BaTiO3.* Nature Communications, 2013. **4**: p. 1808.
[39] Campbell, M.P., J.P.V. McConville, R.G.P. McQuaid, D. Prabhakaran, A. Kumar, and J.M. Gregg, *Hall effect in charged conducting ferroelectric domain walls.* Nature Communications, 2016. **7**: p. 13764.

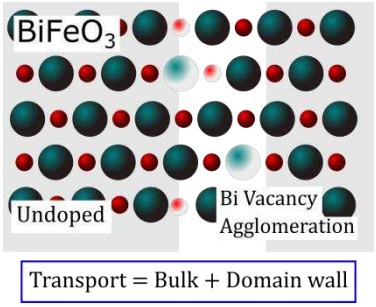

Graphical table of content entry: Electrical transport measurements provide insight into the defect structure of multiferroic $BiFeO_3$.